Wiley Analytical Science

Wiley Analytical Science Virtual Conference

November 9-17

For the 3rd time, The Wiley Analytical Science Conference is back!

It's all happening November 9 - 17

The Wiley Analytical Science Virtual Conference will bring together thousands of researchers and practitioners to share current developments in science and industry. Join for exciting presentations from experts in the fields of analytical and bioanalytical chemistry, pharmaceutical research, materials science, lab automation, and related disciplines.

Register to learn about recent developments & applications in:

- Microscopy
- Spectroscopy
- Mass Spectrometry
- Separation Science
- Much more!

Register here

WILEY

ADVANCED ENERGY MATERIALS
www.advenergymat.de

Luminescence Imaging Characterization of Perovskite Solar Cells: A Note on the Analysis and Reporting the Results

Arman Mahboubi Soufiani, Jincheol Kim, Anita Ho-Baillie, Martin Green, and Ziv Hameiri*

In this essay, the authors use two properly encapsulated high-efficiency mesoscopic perovskite solar cells (PSCs), which use a state-of-the-art perovskite composition $(HC(NH_2)_2PbI_3)_{0.85}(CH_3NH_3PbBr_3)_{0.15}$ with excess PbI_2 as the active layer, to demonstrate the potential effect of dynamical electroluminescence responses on the analysis and interpretation of PSCs electrical characteristic. The essay does not aim to determine how to overcome this issue, nor to investigate its physical/chemical origin, although tentative propositions are made; but rather, to warn researchers in the field about the interpretation and reporting the results obtained from luminescence imaging measurements and the effect of image collection timing on the results. This is a critical message since the authors predict that luminescence imaging techniques will soon become one of the key tools for PSCs characterization, both for long-term stability assessment and fabrication process optimization.

1. Introduction

The rapid progress that has been made in the past seven years in the development of efficient organic–inorganic metal halide (OIMH) perovskite solar cells (PSCs) has created a great excitement among the researchers in the photovoltaic community.[1,2] Power conversion efficiencies beyond 22% is now independently certified.[3] Next constructive steps toward commercialization of PSCs would be to promote our understanding of the device performance limiting factors[4,5] for optimal up-scaling of the PSCs (both in a single- and multijunction configurations[6]) and to overcome the perovskite film and PSCs long-term stability issues.[7–10]

Camera-based photoluminescence (PL) and electroluminescence (EL) imaging techniques, with less than one second image collection times, have been serving the field of silicon solar cells since 2005[11,12] both in research institutes and industrial production lines. Knowledge regarding the information inherent to the PL and EL signals allows one to obtain spatially resolved images of key electrical properties, such as dark saturation current,[13,14] series resistance,[13,15–17] shunt resistance,[18,19] and ideality factor[20] in variety of solar cell structures and throughout the entire production steps. Although popularly used in silicon solar cell and module characterization, these techniques are only at their developing stage in the PSC field.[21–28] They are expected to become one of the dominantly employed techniques in the near future, due to the rapid progress being made in the scaling-up of PSCs for commercialization purposes.

Continuous injection of excess charge-carriers (either optically or electrically) into the perovskite active layer,[29,30] as well as the measurement environmental conditions,[30–32] have been shown to be able to change the electronic properties of perovskites over time, and thus to change the luminescence dynamics of OIMH perovskites.[29,32] As a result, it is not surprising that the luminescence images of PSCs also exhibit transient EL/PL signals, which their dynamics can vary with the device efficiency, the extent of photocurrent hysteresis, and the external bias potential/light intensity during the EL/PL measurements. Due to this temporal behavior of the perovskite semiconductors, either as stand-alone thin film or sandwiched within a full device, there is a genuine concern about the credibility of the consecutive analysis conducted on PL/EL images. In this Essay, we highlight the possible consequential misinterpretation that can be caused by this unfavorable feature of PSCs, regardless of its physical/chemical origin. We examine the current transport efficiency (f_T) images of two devices, fabricated through different methods having similar perovskite composition and device configuration. We demonstrate that for a reliable comparative study of PSCs using luminescence imaging, in particular EL imaging applying an external electric field, it is crucial to consider the temporal electrical response of the devices. This response can considerably vary over time, even under normal measurement conditions.

2. Current Transport Efficiency (f_T)

Wong and Green[33] extended Rau's reciprocity relationship[34] between photovoltaic (external quantum efficiency; EQE_{PV}) and light-emitting diode (EL intensity) operation,[34] to a formalism which allows the assessment of all the current losses occurring in the entire solar cell. Thus, the local current collection

Dr. A. M. Soufiani, J. Kim, Dr. A. Ho-Baillie, Prof. M. Green, Dr. Z. Hameiri
Australian Centre for Advanced Photovoltaics (ACAP)
School of Photovoltaic and Renewable Energy Engineering
University of New South Wales
Sydney 2052, Australia
E-mail: a.mahboubisoufiani@unsw.edu.au

DOI: 10.1002/aenm.201702256

© 2018 WILEY-VCH Verlag GmbH & Co. KGaA, Weinheim

efficiency yields implicit information on the local resistive and recombination losses of the solar cell, accumulated into its fill factor (FF).[35] The newly extended theory incorporates the current (I) and voltage (V_T) at the terminals of the device through[33]

$$f_T(\vec{r}) = \left.\frac{\partial I}{\partial I_L(\vec{r})}\right|_{V_T=0} = \left.\frac{\partial V(\vec{r})}{\partial V_T}\right|_{I_L=0} \quad (1)$$

I_L and V are the photoinduced current collected at the junction and the internal diode voltage at different spatial positions ($\vec{r}$), respectively.[4,33] The last term in Equation (1) allows one to investigate the resistance-limited f_T in the solar cells through EL measurement at incremental V_T changes, assuming that EQE_{PV} is voltage-bias independent.[4] The formalism describing the EL intensity $\varphi_{EL}(E,\vec{r})$ at position $\vec{r}$ and emission energy E is given by[22]

$$\varphi_{EL}(E,\vec{r}) = EQE_{PV}(E,\vec{r})\varphi_{bb}(E)\left[\exp\left(\frac{V(\vec{r})}{V_{th}}\right)-1\right] \quad (2)$$

where $\varphi_{bb}(E)$ is the spectral photon density of a black body and V_{th} is the thermal voltage at the device operating temperature T ($V_{th} = k_b T/q$; k_b is the Boltzmann constant and q is the elementary charge). Reformulating the last term in Equation (1) using Equation (2), for $V(\vec{r}) >> V_{th}$, and integrating over the emission energy range of interest, a readily useable formalism for f_T calculation is obtained

$$f_T(\vec{r}) \approx \frac{\partial \ln(\varphi_{EL}(\vec{r}))}{\partial(V_T)/V_{th}} \quad (3)$$

Through this equation experimental access to the current transport characteristics of a solar cell is obtained by measuring the spatially resolved EL signal upon small incremental change in the terminal voltage. Charge-carrier transport efficiency analysis of solar cells based on this method has been experimentally demonstrated for both single-[4,35,36] and multijunction[37] solar cells.

3. Results

Typical EL images of **Devices A** and **B** captured 20 s after the initiation of the electrical bias are presented in **Figure 1**A,B, while Figure 1E,F show the images 30 s after bias initiation. The images show a noticeable spatial nonuniformity in the devices EL responses, in particular **Device B**. Employing Equation (3), the f_T maps of **Device A** were derived from the images collected at V_T of 1.145 V with incremental voltage of 10 mV. The calculated f_T maps from the images captured 20 and 30 s after the voltage bias initiation are shown in Figure 1C,G, respectively. The f_T maps of **Device B** associated with 20 and 30 s time elapses after voltage biasing at V_T of 1.120 V with incremental voltage of 10 mV are presented in Figure 1D,H. All the EL image measurements were conducted for 35 s in order to minimize potential irreversible effects on the devices and to prevent heating. The PSCs were rested in dark for 3–4 min between each voltage bias soaking.

Arman Mahboubi Soufiani is now with the Australian Centre for Advanced Photovoltaics at the University of New South Wales as a postdoctoral research assistant where he works on the understanding of electrical characteristics and long-term stability of large-area perovskite solar in collaboration with Dr. Ziv Hameiri. He received his Ph.D. at UNSW under the supervision of Professor Martin Green for the fundamental work on investigating the excitonic properties of 3D perovskites and also developing luminescence imaging technique for perovskites characterization.

In **Figure 2**, the distribution of the spatial variation in f_T for different time elapses after bias initiation are presented by histograms. Over time, the f_T peak values shift and the distribution profiles change in both PSCs. However, these changes do not follow a similar trend in the two devices. The generally higher f_T peak value for **Device A** as compared to **Device B** is consistent with the higher FF of the former (see inset tables in **Figure 3**). From these distributions, it can be also seen that the charge-carrier transport efficiency across both devices become more uniform over time, as the f_T distribution profile gets narrower. Additionally, although the solar cells were properly encapsulated, the effect of environmental conditions on these dynamics cannot be fully ruled out. It is worthwhile noting that the conducted measurements presented here were performed on high-efficiency mesoscopic PSCs—(see Figure 3)—and in ambient conditions, which will be common in most laboratories during the characterization sessions, and therefore would not underestimate the significance of the main points intended to be delivered in this Essay.

A closer inspection of the charge-carrier transport efficiency (at two consecutive time elapses) is provided in **Figure 4**. While **Device A** has a narrower f_T distribution after 20 s as compared to **Device B**, its f_T peak value of 0.64 is only slightly higher than that of **Device B** (0.63). However, as mentioned above, the f_T peak position changes over time for the two devices. After 30 s from the voltage bias initiation this difference becomes much larger; f_T peak value shifts to 0.62 for **Device A** and to 0.51 for **Device B**. This evidently shows the significant impact of the image collection timing on the current transport efficiency characteristics of the PSCs, which can greatly affect ones' conclusions when investigating PSCs performance. For these calculations, the device temperatures at all the external voltage biases are assumed to be 300 K. This is based on a recent report characterizing a device working at a similar applied forward bias,[4] where working temperature in the range of 300 ± 3 K was measured. It is worthwhile to note that both devices show a rising behavior in the area-averaged EL intensity over time obtained by averaging the intensity of the EL images

© 2018 WILEY-VCH Verlag GmbH & Co. KGaA, Weinheim

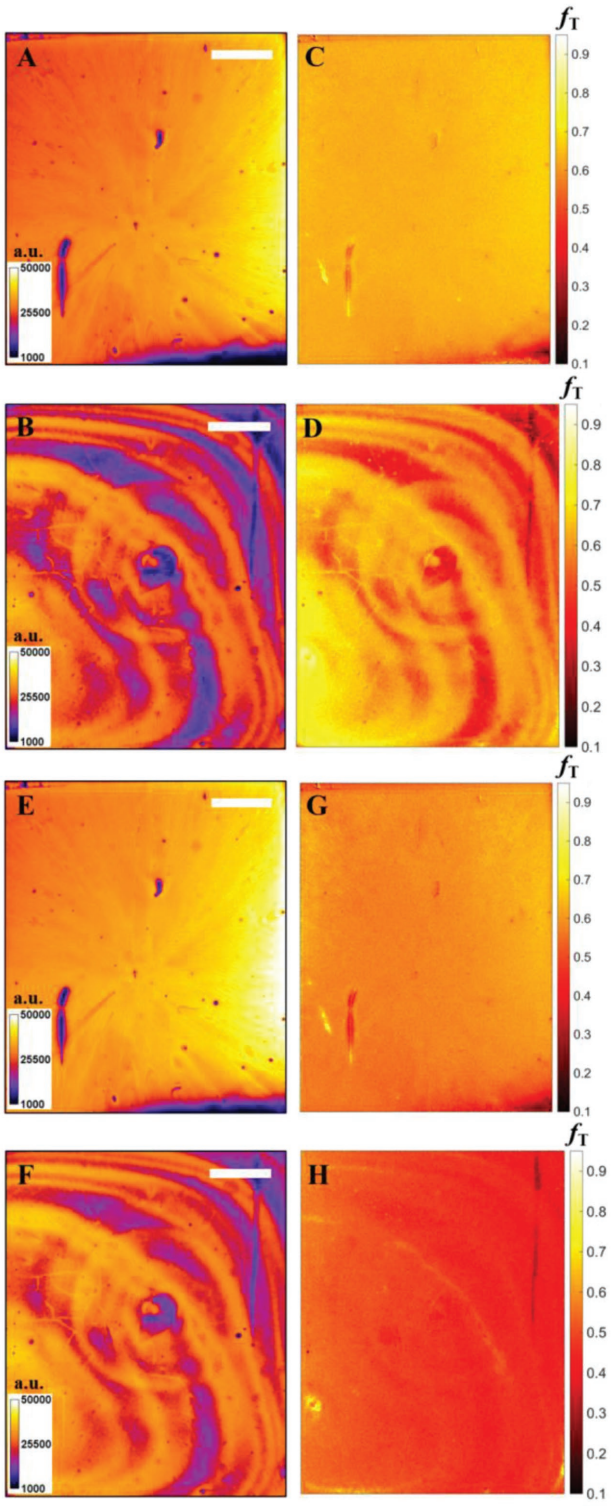

Figure 1. A,B) EL images of **Device A** and **Device B** collected 20 s after voltage bias initiation at $V_T = 1.145$ V and $V_T = 1.120$ V, respectively. C,D) f_T maps calculated for **Device A** and **Device B** 20 s after bias initiation. E,F) EL images of **Device A** and **Device B** collected 30 s after voltage bias initiation at $V_T = 1.145$ V and $V_T = 1.120$ V, respectively. G,H) f_T maps calculated for **Device A** and **Device B** 30 s after bias initiation. The f_T intensities of all the maps are scaled between 0.1 and 0.95. The scale bars are 2 mm.

(see Figure 4C for **Device A** and Figure 4D for **Device B**). We tentatively presume that these observed time-evolving traits can be explained by the possible time-dependent ionic defect transport,[38,39] trap-filling,[40] and interplay of the two[41] upon applying external potential, which may induce changes in the perovskite bulk doping and in the width of the space charge regions. These in turn are expected to reduce the interfacial and/or bulk series resistance and/or decrease the nonradiative recombination current[42] (note Equation (2)), which can result in an EL intensity rise during the forward voltage bias soaking. The observed variation in the f_T peak positions could be, at least to some extent, due to the difference in the rate of transient changes in the underlying electrical/physical mechanisms throughout the bulk/interfaces of the two devices at the two incremental terminal potential biases used for each PSC.

The transient EL response in PSCs could be very slow and remain at its presumably steady-state condition (i.e., when the signal is stabilized) for a narrow timespan, dynamically changing before and after the corresponding plateau.[30] The underlying phenomena contributing to the transient EL signal seems to be the ionic defects migration, dynamically modifying the energy band alignment throughout the device,[24,43] which have been recently shown to occur within timescales of up to 10^3 s in mesoscopic devices with efficiencies above 20%,[44] as opposed to trap-filling phenomenon that happens at much faster timescales. Noting the involvement of both halide anions and organic cations in the ionic transport mechanism,[41,45] with greater activation energies required for the latter, it was proposed that device stabilization for hours might be needed to reach its steady-state working condition.[44]

We have previously reported that in order to be able to validate the generalized Planck's emission law—correlating PL and open-circuit voltage (V_{OC}) of a device—it is necessary to precondition planar $TiO_2/CH_3NH_3PbI_3$-based PSCs through light-soaking.[23] In the same study, the radiative ideality factor extracted from the correlation between EL intensity and junction voltage V approached the desirable value of one, while the reason for the residual mismatch remained unidentified. Based on the current analysis, we can assign this mismatch to the transient nature of the EL signal in a fresh device, which also depicts different dynamics at different external potential biases. The latter effects might have been reduced through light-soaking prior to the image collection, allowing complete validation of the emission law.[23]

Employing a similar approach, the quantitative series resistance of different PSCs after stabilizing their transient PL/V_{OC} was mapped for the first time just recently.[46] Here, we highlight the possibility that methods which require driving solar cells at two operating points[16] or fully EL-based methodologies developed for silicon solar cells,[15] might still suffer from transient effects and their application for PSCs might not be straightforward and require further refinement. It is also not yet clear what could be the impact of the duration of preconditioning process on the EL transient response and therefore on the obtained electrical parameters by luminescence-based imaging methods. Further on this point, it is noteworthy to mention that we have recently shown using luminescence imaging (i.e., via a combination of EL, PL at open-circuit and short-circuit imaging measurements)[24] and through

© 2018 WILEY-VCH Verlag GmbH & Co. KGaA, Weinheim

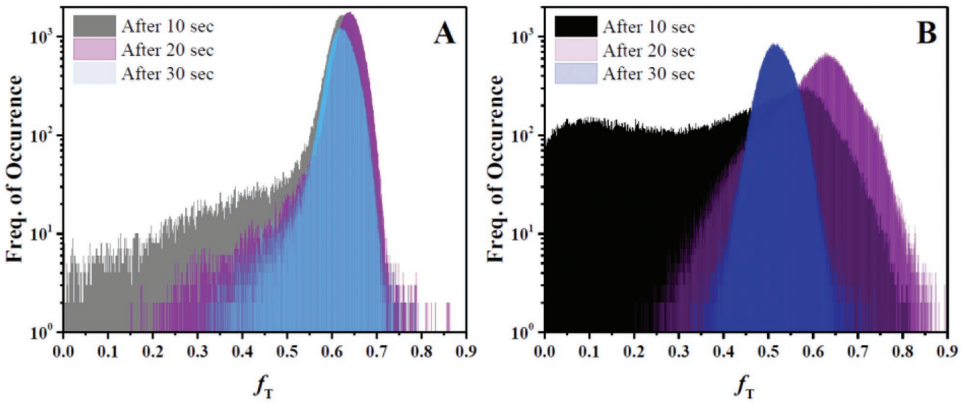

Figure 2. Time evolution of f_T distribution of PSCs. A) Current transport efficiency distribution for **Device A** measured through analysis of two EL images collected at 1.145 and 1.155 V at three different elapse times after bias initiation. B) Current transport efficiency distribution for **Device B** measured through analysis of two EL images collected at 1.120 and 1.130 V at three different elapse times after bias initiation. The lowest of these incremental voltage biases is set to be ≈20 mV higher than the devices open-circuit voltage (see inset tables in Figure 3).

localized light-soaking of $CH_3NH_3PbI_3$-based planar PSCs that one impact of prolonged illumination is a noticeable change in the interfacial series resistance, decreasing it by modifying energy band alignment. Therefore, the preconditioning approach, although innovative and effective in extracting quantitative spatial electrical information for PSCs, needs to be treated cautiously as it may not allow one to gain immediate and accurate information about the as-prepared characteristics of PSCs prepared by various fabrication techniques having similar material constituents.

This Essay highlights some of the difficulties associated with interpretation and reporting measurements obtained by luminescence imaging, in particular through EL imaging of PSCs, even when showing small photocurrent hysteresis. Maintaining the consistency in the timing for the luminescence image collection (i.e., to compare images measured at the same time after switching on the voltage bias) as presented above and also elsewhere[22] might allow for qualitative and comparative studies and quick performance screening of different types of PSCs.

4. Experimental Section

Imaging Setup: The details of the luminescence imaging setup used in this Essay are similar to that described in our previous publications.[22–24] The exposure time used for image collection was 500 ms. The emission from the perovskite layer was collected by a silicon charge coupled device camera within the spectral range of 750–850 nm. All the images were corrected for the dark background offset associated with the readout noise.[15,23] For the purpose of f_T calculations, the EL images were measured at about 20 and 30 mV higher than the devices one Sun V_{OC}.

Mesoscopic PSCs: Two PSCs with compact-TiO_2/mesoporous-TiO_2 as the electron transport layer and Spiro-OMeTAD as the hole transport later were used. The perovskite absorber layer, $(HC(NH_2)_2PbI_3)_{0.85}(CH_3NH_3PbBr_3)_{0.15}$ with excess PbI_2,[47] was deposited onto mesoporous-TiO_2 with two different techniques: spray-assisted (**Device A**) and drop-cast (**Device B**).[48] The devices active area (i.e., gold deposited area) was ≈ 1.2 cm^2. The devices were encapsulated using the polyisobutylene edge-sealed method reported elsewhere,[49] which has proved to be significantly more efficient as a moisture-resistive encapsulant than the simple epoxy edge-sealed method. The obtained efficiencies were in the range of ≈15–16.5% (Figure 3). Both solar cells demonstrated a very small photocurrent hysteresis, in particular **Device A** (see Figure 3). It is

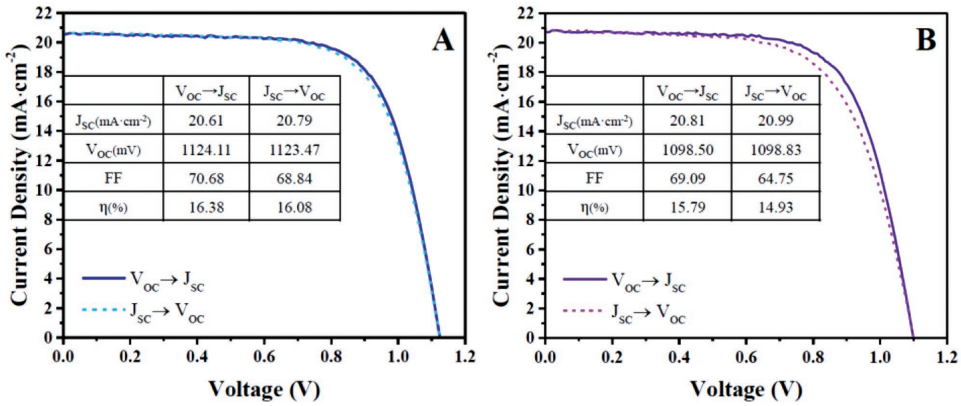

	$V_{OC}\rightarrow J_{SC}$	$J_{SC}\rightarrow V_{OC}$
J_{SC}(mA·cm^{-2})	20.61	20.79
V_{OC}(mV)	1124.11	1123.47
FF	70.68	68.84
η(%)	16.38	16.08

	$V_{OC}\rightarrow J_{SC}$	$J_{SC}\rightarrow V_{OC}$
J_{SC}(mA·cm^{-2})	20.81	20.99
V_{OC}(mV)	1098.50	1098.83
FF	69.09	64.75
η(%)	15.79	14.93

Figure 3. Light current density-voltage curves of **A**) **Device A** and **B**) **Device B** measured both in reverse (solid line) and forward (dashed line) scan directions. The extracted photovoltaic parameters are given in the inset tables. It is noted that the devices were only scanned once in the reverse and forward directions, respectively, without any preconditioning of the devices. The measurements were done at the rate of 100 mV s^{-1}.

© 2018 WILEY-VCH Verlag GmbH & Co. KGaA, Weinheim

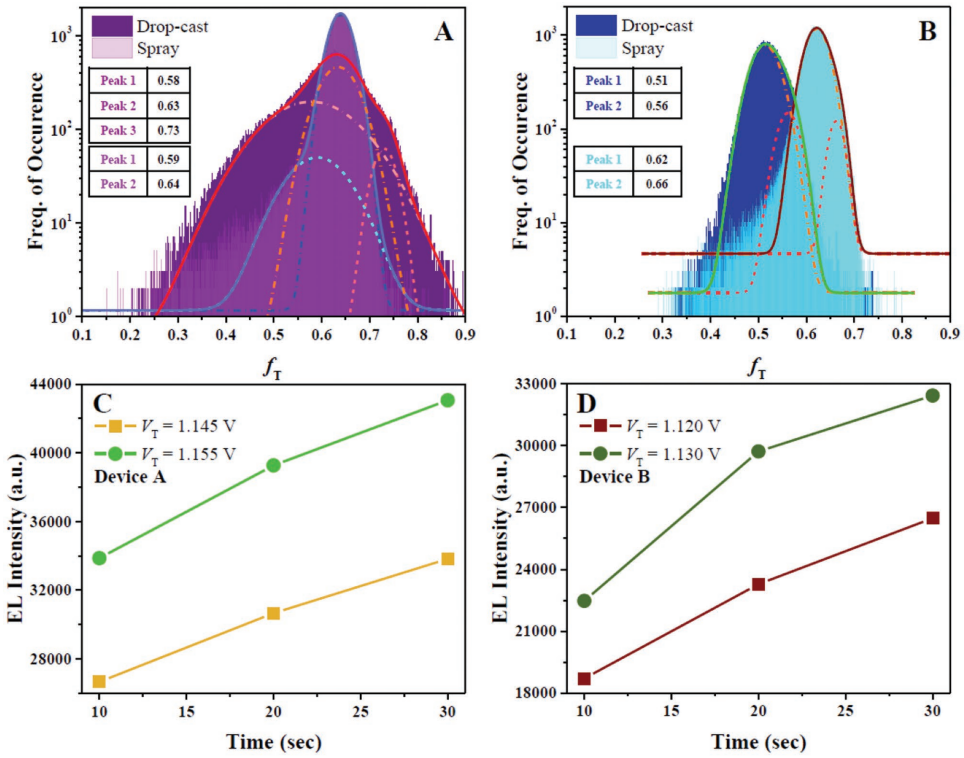

Figure 4. Comparison of f_T distribution of two types of PSCs at a similar time elapse. A) Comparison of the f_T intensity distribution of the two types of devices used in this Essay at the time elapse of 20 s after voltage bias initiation. B) Comparison of the f_T intensity distribution for the two types of devices used in this Essay at the time elapse of 30 s after voltage bias initiation. The distributions are fitted using Gaussian functions and the peak f_T values extracted from the fitting to the profiles are given in the inset tables. C,D) EL dynamics of **Devices A** and **B**, respectively, measured at terminal voltage biases of 20 mV above their V_{OC} with incremental voltage of 10 mV.

worthwhile to note that no preconditioning was conducted prior to the light current density–voltage (*J*–*V*) characterizations of these solar cells.

Acknowledgements

The authors acknowledge support from the Australian Government through the Australian Renewable Energy Agency (ARENA; Grant 2014/RND097), the Australian Research Council (ARC; Grant DE150100268) and the Australian Centre for Advanced Photovoltaics (ACAP). The views expressed herein are not necessarily the views of the Australian Government, and the Australian Government does not accept responsibility for any information or advice contained herein.

Conflict of Interest

The authors declare no conflict of interest.

Keywords

electroluminescence imaging, perovskite solar cells, transient electrical responses

Received: August 17, 2017
Revised: November 21, 2017
Published online: January 26, 2018

[1] M. A. Green, A. Ho-Baillie, *ACS Energy Lett.* **2017**, *2*, 822.
[2] M. A. Green, A. Ho-Baillie, H. J. Snaith, *Nat. Photonics* **2014**, *8*, 506.
[3] W. S. Yang, B.-W. Park, E. H. Jung, N. J. Jeon, Y. C. Kim, D. U. Lee, S. S. Shin, J. Seo, E. K. Kim, J. H. Noh, S. I. Seok, *Science* **2017**, *356*, 1376.
[4] G. El-Hajje, C. Momblona, L. Gil-Escrig, J. Ávila, T. Guillemot, J.-F. Guillemoles, M. Sessolo, H. J. Bolink, L. Lombez, *Energy Environ. Sci.* **2016**, *9*, 2286.
[5] Q. Lin, R. C. R. Nagiri, P. L. Burn, P. Meredith, *Adv. Opt. Mater.* **2017**, *5*, 1600819.
[6] A. Priyadarshi, L. J. Haur, P. Murray, D. Fu, S. Kulkarni, G. Xing, T. C. Sum, N. Mathews, S. G. Mhaisalkar, *Energy Environ. Sci.* **2016**, *9*, 3687.
[7] G. Grancini, C. Roldán-Carmona, I. Zimmermann, E. Mosconi, X. Lee, D. Martineau, S. Narbey, F. Oswald, F. De Angelis, M. Graetzel, M. K. Nazeeruddin, *Nat. Commun.* **2017**, *8*, 15684.
[8] J. Lu, L. Jiang, W. Li, F. Li, N. K. Pai, A. D. Scully, C.-M. Tsai, U. Bach, A. N. Simonov, Y.-B. Cheng, L. Spiccia, *Adv. Energy Mater.* **2017**, *7*, 1700444.
[9] E. L. Unger, E. T. Hoke, C. D. Bailie, W. H. Nguyen, A. R. Bowring, T. Heumüller, M. G. Christoforo, M. D. McGehee, *Energy Environ. Sci.* **2014**, *7*, 3690.
[10] Y. Lin, Y. Bai, Y. Fang, Q. Wang, Y. Deng, J. Huang, *ACS Energy Lett.* **2017**, *2*, 1571.
[11] T. Fuyuki, H. Kondo, T. Yamazaki, Y. Takahashi, Y. Uraoka, *Appl. Phys. Lett.* **2005**, *86*, 262108.
[12] T. Trupke, R. A. Bardos, M. C. Schubert, W. Warta, *Appl. Phys. Lett.* **2006**, *89*, 044107.

© 2018 WILEY-VCH Verlag GmbH & Co. KGaA, Weinheim

[13] M. Glatthaar, J. Haunschild, M. Kasemann, J. Giesecke, W. Warta, S. Rein, *Phys. Status Solidi RRL* **2010**, *4*, 13.
[14] Z. Hameiri, P. Chaturvedi, *Appl. Phys. Lett.* **2013**, *102*, 073502.
[15] J. Haunschild, M. Glatthaar, M. Kasemann, S. Rein, E. R. Weber, *Phys Status Solidi RRL* **2009**, *3*, 227.
[16] H. Kampwerth, T. Trupke, J. W. Weber, Y. Augarten, *Appl. Phys. Lett.* **2008**, *93*, 202102.
[17] D. Hinken, K. Ramspeck, K. Bothe, B. Fischer, R. Brendel, *Appl. Phys. Lett.* **2007**, *91*, 182104.
[18] M. Kasemann, D. Grote, B. Walter, W. Kwapil, T. Trupke, Y. Augarten, R. A. Bardos, E. Pink, M. D. Abbott, W. Warta, *Prog. Photovoltaics* **2008**, *16*, 297.
[19] O. Breitenstein, J. Bauer, T. Trupke, R. A. Bardos, *Prog. Photovoltaics* **2008**, *16*, 325.
[20] Z. Hameiri, P. Chaturvedi, K. R. McIntosh, *Appl. Phys. Lett.* **2013**, *103*, 023501.
[21] M. Okano, M. Endo, A. Wakamiya, M. Yoshita, H. Akiyama, Y. Kanemitsu, *Appl. Phys. Express* **2015**, *8*, 102302.
[22] A. M. Soufiani, M. J. Y. Tayebjee, S. Meyer, A. Ho-Baillie, J. Sung Yun, R. W. MacQueen, L. Spiccia, M. A. Green, Z. Hameiri, *J. Appl. Phys.* **2016**, *120*, 035702.
[23] Z. Hameiri, A. Mahboubi Soufiani, M. K. Juhl, L. Jiang, F. Huang, Y.-B. Cheng, H. Kampwerth, J. W. Weber, M. A. Green, T. Trupke, *Prog. Photovoltaics* **2015**, *23*, 1697.
[24] A. M. Soufiani, Z. Hameiri, S. Meyer, S. Lim, M. J. Y. Tayebjee, J. S. Yun, A. Ho-Baillie, G. J. Conibeer, L. Spiccia, M. A. Green, *Adv. Energy Mater.* **2017**, *7*, 1602111.
[25] L. E. Mundt, F. D. Heinz, S. Albrecht, M. Mundus, M. Saliba, J. P. Correa-Baena, E. H. Anaraki, L. Korte, M. Grätzel, A. Hagfeldt, B. Rech, M. C. Schubert, S. W. Glunz, *IEEE J. Photovoltaics* **2017**, *7*, 1081.
[26] S. Mastroianni, F. D. Heinz, J.-H. Im, W. Veurman, M. Padilla, M. C. Schubert, U. Würfel, M. Grätzel, N.-G. Park, A. Hinsch, *Nanoscale* **2015**, *7*, 19653.
[27] Y. Wu, H. Shen, D. Walter, D. Jacobs, T. Duong, J. Peng, L. Jiang, Y.-B. Cheng, K. Weber, *Adv. Funct. Mater.* **2016**, *26*, 6807.
[28] H. Shen, Y. Wu, J. Peng, T. Duong, X. Fu, C. Barugkin, T. P. White, K. Weber, K. R. Catchpole, *ACS Appl. Mater. Interfaces* **2017**, *9*, 5974.
[29] D. W. deQuilettes, W. Zhang, V. M. Burlakov, D. J. Graham, T. Leijtens, A. Osherov, V. Bulović H. J. Snaith, D. S. Ginger, S. D. Stranks, *Nat. Commun.* **2016**, *7*, 11683.
[30] O. A. Jaramillo-Quintero, R. S. Sanchez, M. Rincon, I. Mora-Sero, *J. Phys. Chem. Lett.* **2015**, *6*, 1883.
[31] Y. Tian, A. Merdasa, E. Unger, M. Abdellah, K. Zheng, S. McKibbin, A. Mikkelsen, T. Pullerits, A. Yartsev, V. Sundström, I. G. Scheblykin, *J. Phys. Chem. Lett.* **2015**, *6*, 4171.
[32] H.-H. Fang, S. Adjokatse, H. Wei, J. Yang, G. R. Blake, J. Huang, J. Even, M. A. Loi, *Sci. Adv.* **2016**, *2*, e1600534.
[33] J. Wong, M. A. Green, *Phys. Rev. B* **2012**, *85*, 235205.
[34] U. Rau, *Phys. Rev. B* **2007**, *76*, 085303.
[35] U. Rau, V. Huhn, L. Stoicescu, M. Schneemann, Y. Augarten, A. Gerber, B. E. Pieters, *Appl. Phys. Lett.* **2014**, *105*, 163507.
[36] J. Wong, R. Sridharan, Y. C. Wang, T. Mueller, presented at *40th IEEE Photovoltaic Specialist Conf. (PVSC) 2014*, Colorado Convention Center, Denver, CO, USA, June **2014**.
[37] A. Delamarre, J. Jia, P. Verdier, K. Watanabe, M. Sugiyama, Y. Nakano, J.-F. Guillemoles, *Proc. SPIE* **2017**, 10099, 100990Z.
[38] C. Eames, J. M. Frost, P. R. F. Barnes, B. C. O'Regan, A. Walsh, M. Islam, *Nat. Commun.* **2015**, *6*, 7497.
[39] S. Meloni, T. Moehl, W. Tress, M. Franckevičius, M. Saliba, Y. H. Lee, P. Gao, M. K. Nazeeruddin, S. M. Zakeeruddin, U. Rothlisberger, M. Graetzel, *Nat. Commun.* **2016**, *7*, 10334.
[40] S. D. Stranks, *ACS Energy Lett.* **2017**, *2*, 1515.
[41] W. Tress, *J. Phys. Chem. Lett.* **2017**, *8*, 3106.
[42] T. M. H. Tran, B. E. Pieters, C. Ulbrich, A. Gerber, T. Kirchartz, U. Rau, *Thin Solid Films* **2013**, *535*, 307.
[43] R. A. Belisle, W. H. Nguyen, A. R. Bowring, P. Calado, X. Li, S. J. C. Irvine, M. D. McGehee, P. R. F. Barnes, B. C. O'Regan, *Energy Environ. Sci.* **2017**, *10*, 192.
[44] K. Domanski, B. Roose, T. Matsui, M. Saliba, S.-H. Turren-Cruz, J.-P. Correa-Baena, C. R. Carmona, G. Richardson, J. M. Foster, F. De Angelis, J. M. Ball, A. Petrozza, N. Mine, M. K. Nazeeruddin, W. Tress, M. Grätzel, U. Steiner, A. Hagfeldt, A. Abate, *Energy Environ. Sci.* **2017**, *10*, 604.
[45] Y. Yuan, J. Huang, *Acc. Chem. Res.* **2016**, *49*, 286.
[46] D. Walter, Y. Wu, T. Duong, J. Peng, L. Jiang, K. C. Fong, K. Weber, *Adv. Energy Mater.* **2017**, *8*, 1701522.
[47] Y. C. Kim, N. J. Jeon, J. H. Noh, W. S. Yang, J. Seo, J. S. Yun, A. Ho-Baillie, S. Huang, M. A. Green, J. Seidel, T. K. Ahn, S. I. Seok, *Adv. Energy Mater.* **2016**, *6*, 1502104.
[48] J. Kim, J. S. Yun, Y. Cho, D. S. Lee, B. Wilkinson, A. M. Soufiani, X. Deng, J. Zheng, A. Shi, S. Lim, S. Chen, Z. Hameiri, M. Zhang, C. F. J. Lau, S. Huang, M. A. Green, A. W. Y. Ho-Baillie, *ACS Energy Lett.* **2017**, *2*, 1978.
[49] L. Shi, T. L. Young, J. Kim, Y. Sheng, L. Wang, Y. Chen, Z. Feng, M. J. Keevers, X. Hao, P. J. Verlinden, M. A. Green, A. W. Y. Ho-Baillie, *ACS Appl. Mater. Interfaces* **2017**, *9*, 25073.

© 2018 WILEY-VCH Verlag GmbH & Co. KGaA, Weinheim